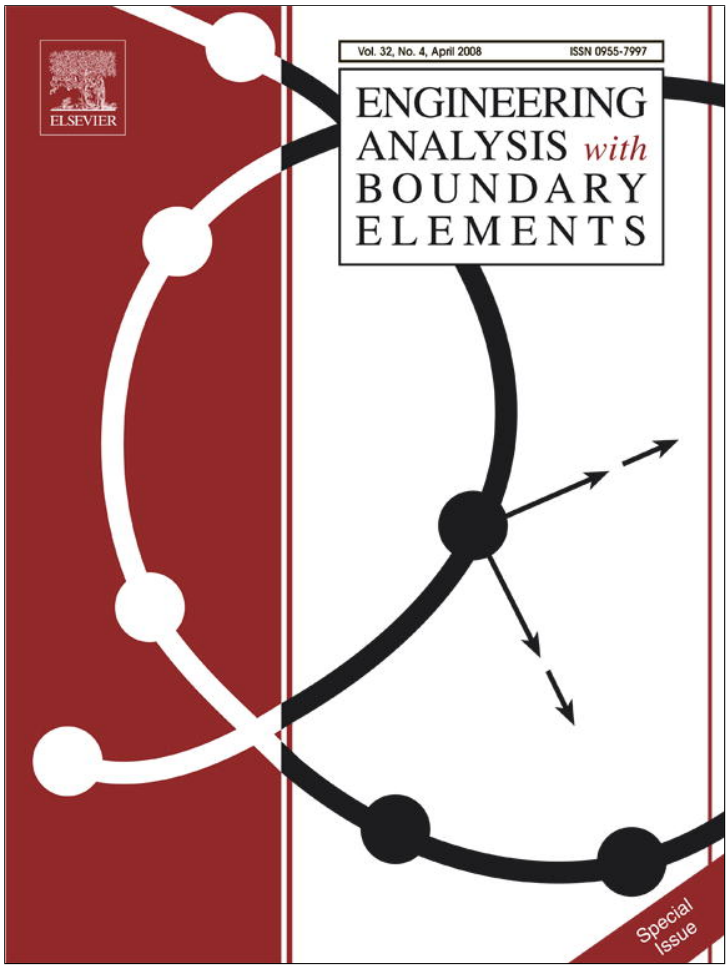

ELSEVIER

Engineering Analysis with Boundary Elements 32 (2008) 328–335

ENGINEERING ANALYSIS with BOUNDARY ELEMENTS

www.elsevier.com/locate/enganabound

BEM calculation of strain energy density and relative strain energy in QWR nanostructures

E. Pan[a,b,*], Y. Zhang[a,b], P.W. Chung[c]

[a]Department of Civil Engineering, University of Akron, Akron, OH 44325, USA
[b]Department of Applied Mathematics, University of Akron, Akron, OH 44325, USA
[c]U.S. Army Research Laboratory, Aberdeen Proving Ground, MD 21005, USA

Received 20 February 2007; accepted 13 July 2007
Available online 4 March 2008

Abstract

In this paper, we propose a bimaterial boundary element method (BEM) for the calculation of the strain energy density and the relative strain energy in quantum wire (QWR) nanostructures. We first derive the bimaterial Green's functions in terms of the Stroh formalism. We then discretize the boundary of the problem with constant elements for which the involved Green's function kernels can be exactly integrated. Our bimaterial BEM program is finally applied to calculate the strain energy density and relative strain energy in free-standing/embedded InAs QWR on/in GaAs substrate. For a square InAs (1 1 1) QWR, it is found that the magnitude of the relative strain energy increases with increasing depth of the QWR with respect to the surface of the GaAs (1 1 1) substrate. For an isosceles triangle of InAs (1 1 1) QWR free-standing on the surface of the GaAs (1 1 1) substrate, we found that the magnitude of the relative strain energy increases with increasing base angle of the triangle QWR. Strain energy density inside the InAs QWR is also plotted to show its strong dependence on the QWR shape. These results could be useful to the control of the QWR shape and size in epitaxial growth

Keywords: BEM; QWR; Bimaterial; Green's function; Strain energy; Stroh formalism; InAs; GaAs

1. Introduction

Quantum wire (QWR) semiconductor nanostructures and their quantum-mechanical properties have been the subjects of intensive study during the past decade [1,2]. Ross et al. studied the quantum dots (QDs) coarsening in the presence of a shape transition [3]. Medeiros-Ribeiro et al. also investigated the shape transition of the Ge nanocrystals on Si (0 0 1) surface from pyramids to domes. Daruka et al. further analyzed the equilibrium shape of strained islands and showed that the QWR shape varies with its size [4]. Analytical approaches have been proposed for the strain and electric field analyses in QWRs embedded semiconductor substrates, e.g. [5]. It has been shown more recently that Green's functions and boundary element methods (BEMs) possess various advantages over the domain-discretization methods [6,7]. However, for the free-standing QWR case and particularly for a QWR within a bimaterial substrate, the corresponding bimaterial BEM is required. Even though the free-standing QWR case could also be analyzed by a BEM formulation based on the half-plane Green's function, the bimaterial approach offers more generality and flexibility.

Two-dimensional (2D) BEM is very convenient in analyzing stress and fracture problems in bimaterial solids. The bimaterial Green's functions in transversely isotropic piezoelectric solids [8], anisotropic elastic [9] and piezoelectric bodies [10–12], and in magnetoelectroelastic solids [13] were studied and applied to different mechanical and piezoelectric problems. We remark that these Green's functions were presented in the Lekhnitskii formalism (e.g., [9]). Applications of the 2D BEM also include the determination of stress intensity factors for interfacial rigid line inclusion [14], symmetric BEM formulation for cohesive interface problem [15], and analysis of collinear interfacial cracks interaction [16]. Another extended studies

*Corresponding author at: Department of Civil Engineering, University of Akron, Akron, OH 44325, USA.
E-mail address: pan2@uakron.edu (E. Pan).

0955-7997/$ - see front matter © 2007 Elsevier Ltd. All rights reserved.
doi:10.1016/j.enganabound.2007.07.009

include thermomechanical closure of interfacial cracks [17], fracture problems in magnetoelectroelastic composites [18], and dynamic fracture problems involving bimaterial solids [19–21].

In this paper, we develop the anisotropic bimaterial Green's functions in terms of the efficient and powerful Stroh formalism [22] and the corresponding BEM program for the analysis of the strain energy density and the relative strain energy for a QWR free-standing on or embedded in an anisotropic semiconductor substrate. To treat the misfit lattice eigenstrain within the QWR, we first convert the associated area integral to a line integral along the interface of the QWR and its substrate. Then we discretize the boundary with constant elements so that the involved kernel integration can be carried out in an exact closed form, which is solved for the boundary (interface) values. The induced elastic field inside and outside the QWR can be obtained using the solved interface values. We remark that in order to apply our bimaterial program to the free-standing QWR case, we only need to assume that the material stiffness in the upper half-plane is much smaller than that in the lower half-plane substrate.

Our bimaterial BEM program is first tested against various existing results. It is then applied to calculate the strain energy density and the relative strain energy in the InAs (1 1 1) QWR which is free-standing on or embedded in the GaAs substrate. Our numerical results show that, for the case of an isosceles triangle QWR on the substrate, the strain energy density within the QWR strongly depends on the base angle of the triangle. We also observe that the magnitude of the relative strain energy for this case increases with increasing side angle. For a square QWR either free-standing on or embedded in the substrate, we found that the magnitude of the relative strain energy increases with increasing depth of the QWR to the substrate surface. Our numerical examples demonstrate the significant influence of the QWR shape and the QWR location on both the strain energy density and the relative strain energy in the QWR, which should be particularly useful to the successful growth of QWRs via epitaxial approach.

This paper is organized as follows: In Section 2, the basic equations are presented. In Section 3, the boundary integral equation and the required four sets of Green's functions for the bimaterial matrix are presented, including also the formulation of elastic strain energy density and the relative strain energy. Numerical examples are presented in Section 4, and conclusions are drawn in Section 5.

2. Problem description

We assume that there is a QWR of arbitrary shape within a bimaterial substrate. A uniform eigenstrain γ^*_{ij} field is applied inside the QWR as shown in Fig. 1. The elastic moduli in the QWR, material 1, and material 2 are denoted, respectively, as c^w_{ijkl}, c^1_{ijkl}, and c^2_{ijkl}.

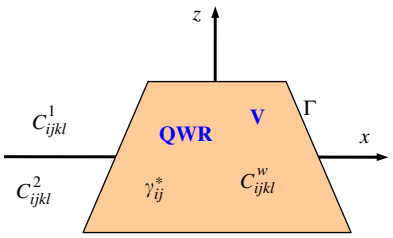

Fig. 1. A general QWR within a bimaterial substrate: an eigenstrain γ^*_{ij} is applied to the QWR which is an arbitrarily shaped polygon.

In each domain, the constitutive relation can be written as

$$\sigma_{ij} = C_{ijkl}\gamma_{kl}, \tag{1}$$

where γ_{ij} is the strain, σ_{ij} the stress, and C_{ijkl} the elastic stiffness.

The strain–displacement relation for small deformation is

$$\gamma_{ij} = 0.5(u_{i,j} + u_{j,i}), \tag{2}$$

where u_i is the elastic displacement.

The total strain can be written as

$$\gamma_{ij} = \gamma^e_{ij} + \gamma^*_{ij}, \tag{3}$$

where γ^e_{ij} is the strain as shown in the constitutive relation.

Substituting (3) into (1), we have

$$\sigma_{ij} = C_{ijkl}(\gamma_{kl} - \chi\gamma^*_{kl}), \tag{4}$$

where χ is equal to 1 if the field point is within the QWR domain V and to 0 otherwise (Fig. 1).

Therefore, substituting Eq. (4) into the equilibrium equation of zero body force

$$\sigma_{ij,i} = 0 \tag{5}$$

results in

$$C_{ijkl}u_{k,li} - \chi C^w_{ijkl}\gamma^*_{kl,i} = 0, \tag{6}$$

where the second term in Eq. (6) is the equivalent body force of the eigenstrain in the QWR domain defined as [23,24]

$$f^{(w)}_j = -C^w_{ijkl}\gamma^*_{kl,i}. \tag{7}$$

3. Boundary integral equations and bimaterial Green's functions

3.1. Boundary integral equations

The boundary integral formulation can be expressed as

$$b_{ij}(\boldsymbol{X})u^{(m)}_j(\boldsymbol{X}) = \int_\Gamma [U^{(m)}_{ij}(\boldsymbol{X},\boldsymbol{x})t^{(m)}_j(\boldsymbol{x}) - T^{(m)}_{ij}(\boldsymbol{X},\boldsymbol{x})u^{(m)}_j(\boldsymbol{x})]\,\mathrm{d}\Gamma(\boldsymbol{x}) \tag{8}$$

for the matrix (or substrate), and

$$b_{ij}(\boldsymbol{X})u^{(w)}_j(\boldsymbol{X}) = \int_\Gamma \{U^{(w)}_{ij}(\boldsymbol{X},\boldsymbol{x})[t^{(w)}_j(\boldsymbol{x}) + t^{(fw)}_j(\boldsymbol{x})] - T^{(w)}_{ij}(\boldsymbol{X},\boldsymbol{x})u^{(w)}_j(\boldsymbol{x})\}\,\mathrm{d}\Gamma(\boldsymbol{x}) \tag{9}$$

for the QWR. The superscripts (m) and (w) denote the quantities with respect to the matrix (substrate) and QWR, respectively. In Eqs. (8) and (9), $\boldsymbol{X}$ and $\boldsymbol{x}$ stand for the source and field points, respectively, U_{ij} and T_{ij} are the displacement and traction Green's functions, respectively. u_i and t_i are the displacement and traction components along the boundary. The coefficient b_{ij} is equal to δ_{ij} if the source point $\boldsymbol{X}$ is an interior point and $\delta_{ij}/2$ if $\boldsymbol{X}$ is at a smooth boundary. $t_j^{(fw)}$ is the traction associated with the misfit eigenstrain inside the QWR, obtained from Eq. (7), as $t_j^{(fw)} = -C_{ijkl}^{w}\gamma_{kl}^{*}n_i$, with n_i being the outward normal of the boundary.

We now divide the boundary into N constant elements, resulting in the discretized boundary integral equations

$$b_{ij}u_j^{(m)} + \sum_{n=1}^{N}\left(\int_{\Gamma_n} T_{ij}^{(m)}\,\mathrm{d}\Gamma\right)u_{jn} = \sum_{n=1}^{N}\left(\int_{\Gamma_n} U_{ij}^{(m)}\,\mathrm{d}\Gamma\right)t_{jn} \quad (10)$$

for the matrix (substrate), and

$$b_{ij}u_j^{(w)} + \sum_{n=1}^{N}\left(\int_{\Gamma_n} T_{ij}^{(w)}\,\mathrm{d}\Gamma\right)u_{jn} = \sum_{n=1}^{N}\left(\int_{\Gamma_n} U_{ij}^{(w)}\,\mathrm{d}\Gamma\right)(t_{jn} + C_{ijkl}^{(w)}\gamma_{kl}^{*}n_j) \quad (11)$$

for the QWR. In Eqs. (10) and (11), u_{jn} and t_{jn} are the center values on the nth element.

3.2. Bimaterial Green's functions

It is noted that in order to solve the discretized boundary integral equations (10) and (11), the involved Green's functions U_{ij} and T_{ij} and their integrations on each element are required. These are presented below.

In the boundary integral equation (11) for the QWR domain, only the full-plane Green's functions are required, which can be expressed as [25]

$$U_{jk}(\boldsymbol{X},\boldsymbol{x}) = \frac{1}{\pi}\mathrm{Im}\{A_{jr}\ln(z_r - s_r)A_{kr}\} \quad (12)$$

for the displacement, and

$$T_{jk}(\boldsymbol{X},\boldsymbol{x}) = -\frac{1}{\pi}\mathrm{Im}\left\{B_{jr}\frac{p_r n_1 - n_3}{z_r - s_r}A_{kr}\right\} \quad (13)$$

for the traction. In Eqs. (12) and (13), n_1 and n_3 are the outward normal components at point $\boldsymbol{x}$, and the complex variables z_r and s_r $(r = 1,2,3)$ are defined by

$$z_r = x + p_r z \quad (14)$$

and

$$s_r = X + p_r Z. \quad (15)$$

In Eqs. (14) and (15), p_r $(r = 1,2,3)$ are the eigenvalues of the QWR material, which are related to the elastic moduli only, and $\boldsymbol{A}$ and $\boldsymbol{B}$ are the corresponding eigenmatrices [22,25].

For the matrix domain (i.e., the bimaterial substrate), due to the relative locations of the source and field points, there are four sets of Green's functions. Again, these Green's functions were derived in terms of the Lekhnitskii formalism, e.g., by Pan [10]. However, the Stroh formalism is more convenient and efficient [22]. Therefore, we first present these bimaterial Green's functions in the Stroh formalism. We refer to Fig. 1 where materials 1 and 2 occupy the half-plane $z>0$ and $z<0$, respectively.

First, let the source point $\boldsymbol{X} = (X,Z)$ be in material 1 $(z>0)$. Then, if the field point $\boldsymbol{x} = (x,z)$ is in the $z>0$ half-plane, the displacement and traction Green's functions can be expressed as

$$U_{kj}^{1} = \frac{1}{\pi}\mathrm{Im}\left\{A_{jr}^{1}\ln(z_r - s_r)A_{kr}^{1} + \sum_{v=1}^{3}[A_{jr}^{1}\ln(z_r - \bar{s}_v)Q_{rk}^{11,v}]\right\}, \quad (16)$$

$$T_{kj}^{1} = -\frac{1}{\pi}\mathrm{Im}\left\{B_{jr}^{1}\frac{p_r^1 n_1 - n_3}{z_r - s_r}A_{kr}^{1} + \sum_{v=1}^{3}\left[B_{jr}^{1}\frac{p_r^1 n_1 - n_3}{z_r - \bar{s}_v}Q_{rk}^{11,v}\right]\right\}. \quad (17)$$

On the other hand, if the field point is in the $z<0$ half-plane, then

$$U_{kj}^{2} = \frac{1}{\pi}\mathrm{Im}\sum_{v=1}^{3}[A_{jr}^{2}\ln(z_r - s_v)Q_{rk}^{12,v}], \quad (18)$$

$$T_{kj}^{2} = -\frac{1}{\pi}\mathrm{Im}\sum_{v=1}^{3}\left[B_{jr}^{2}\frac{p_r^2 n_1 - n_3}{z_r - s_v}Q_{rk}^{12,v}\right]. \quad (19)$$

Now, let the source point (X,Z) be in material 2 $(z<0)$. Then, if the field point (x,z) is in the $z>0$ half-plane, we have

$$U_{kj}^{1} = \frac{1}{\pi}\mathrm{Im}\sum_{v=1}^{3}[A_{jr}^{1}\ln(z_r - s_v)Q_{rk}^{21,v}], \quad (20)$$

$$T_{kj}^{1} = -\frac{1}{\pi}\mathrm{Im}\sum_{v=1}^{3}\left[B_{jr}^{1}\frac{p_r^1 n_1 - n_3}{z_r - s_v}Q_{rk}^{21,v}\right]. \quad (21)$$

On the other hand, if the field point is in the $z<0$ half-plane,

$$U_{kj}^{2} = \frac{1}{\pi}\mathrm{Im}\left\{A_{jr}^{2}\ln(z_r - s_r)A_{kr}^{2} + \sum_{v=1}^{3}[A_{jr}^{2}\ln(z_r - \bar{s}_v)Q_{rk}^{22,v}]\right\}, \quad (22)$$

$$T_{kj}^{2} = -\frac{1}{\pi}\mathrm{Im}\left\{B_{jr}^{2}\frac{p_r^2 n_1 - n_3}{z_r - s_r}A_{kr}^{2} + \sum_{v=1}^{3}\left[B_{jr}^{2}\frac{p_r^2 n_1 - n_3}{z_r - \bar{s}_v}Q_{rk}^{22,v}\right]\right\}. \quad (23)$$

In Eqs. (16)–(23), the superscript 1 or 2 to p, $\boldsymbol{A}$, and $\boldsymbol{B}$, denotes that these eigenvalues and the corresponding eigenmatrices belong to material 1 or 2. The matrix $\boldsymbol{Q}$ depends on the relative locations of the source and field points, and its expression is given in Appendix A.

3.3. Integration of infinite-plane and bimaterial Green's functions

In order to carry out the line integral of the involved Green's functions over each constant element (e.g., along the nth element Γ_n), we let the generic element start from point 1 (x_1, z_1) and end at point 2 (x_2, z_2), with length $l = \sqrt{(x_2 - x_1)^2 + (z_2 - z_1)^2}$. Then, the integration of the involved Green's displacements and tractions (only the integral variable-dependent function) for the QWR (which requires only the infinite-plane Green's functions) can be expressed as

$$\begin{aligned} h_r(x,z) &= \int_{\Gamma_n} \ln(z_r - s_r)\,\mathrm{d}\Gamma_n \\ &= l\left[\frac{(x_1 + p_r z_1) - s_r}{(x_2 - x_1) + p_r(z_2 - z_1)} \ln\left[\frac{(x_2 + p_r z_2) - s_r}{(x_1 + p_r z_1) - s_r}\right] \right. \\ &\quad \left. + \ln(x_2 + p_r z_2 - s_r) - 1\right], \end{aligned} \tag{24}$$

$$\begin{aligned} g_r(x,z) &= \int_{\Gamma_n} \frac{1}{z_r - s_r}\,\mathrm{d}\Gamma_n \\ &= l\left[\frac{1}{(x_2 - x_1) + p_r(z_2 - z_1)} \ln\left(\frac{x_2 + p_r z_2 - s_r}{x_1 + p_r z_1 - s_r}\right)\right]. \end{aligned} \tag{25}$$

We point out that similar expressions can be found for the integration of the bimaterial Green's functions in the substrate.

3.4. Derivatives of infinite-plane and bimaterial Green's functions

In order to obtain the strain and stress fields, we also need to take the derivative of Green's displacement and traction with respect to the source point, and then find the corresponding integration. The integration of the involved Green's function derivatives for the QWR domain can be written as

$$\begin{aligned} h_{r,x} &= \int_{\Gamma_n} \frac{\partial \ln(z_r - s_r)}{\partial x}\,\mathrm{d}\Gamma_n \\ &= -\frac{l}{(x_2 - x_1) + p_r(z_2 - z_1)} \ln\left(\frac{x_2 + p_r z_2 - s_r}{x_1 + p_r z_1 - s_r}\right), \end{aligned} \tag{26}$$

$$h_{r,z} = p_r h_{r,x}, \tag{27}$$

$$\begin{aligned} g_{r,x} &= \int_{\Gamma_n} \frac{\partial}{\partial x}\frac{1}{z_r - s_r}\,\mathrm{d}\Gamma_n \\ &= \frac{l}{(x_2 - x_1) + p_r(z_2 - z_1)} \\ &\quad \times \left[-\frac{1}{x_2 + p_r z_2 - s_r} + \frac{1}{x_1 + p_r z_1 - s_r}\right], \end{aligned} \tag{28}$$

$$g_{r,z} = p_r g_{r,x}. \tag{29}$$

Again, similar expressions can be found for the corresponding bimaterial substrate.

3.5. Strain energy density and relative strain energy

During growth of QWR nanostructures, strain energy in the QWR plays an important role. Therefore, its calculation and prediction are of great interest. Following [23], the strain energy in the QWR can be expressed as

$$W = \frac{1}{2}\int_V \sigma_{ij}(\gamma_{ij} - \gamma^*_{ij})\,\mathrm{d}V. \tag{30}$$

We remark that the integrand $\frac{1}{2}\sigma_{ij}(\gamma_{ij} - \gamma^*_{ij})$ is the strain energy density within the QWR, which will be also calculated and studied.

Applying the Gauss divergence theorem and assuming that the eigenstrain is uniform inside the QWR, the total elastic strain energy of QWR in Eq. (30) can be expressed alternatively as

$$W = \frac{1}{2}\int_\Gamma t_i u_i\,\mathrm{d}\Gamma - \frac{1}{2}\int_\Gamma t_k^{(fw)} u_k\,\mathrm{d}\Gamma + \frac{1}{2}\int_V C_{ijkl}\gamma^*_{ij}\gamma^*_{kl}\,\mathrm{d}V, \tag{31}$$

where Γ is the boundary of QWR. While the first boundary integration on the right-hand side of Eq. (31) represents the work done by the traction acting on the boundary, the second boundary integration represents the work done by the traction associated with the eigenstrain as we recall that $t_k^{(fw)} = C_{ijkl}\gamma^*_{ij}n_l$. The last volumetric integration corresponds to the initial constant strain energy of the eigenstrain field, i.e., the constant strain energy in the wetting layer (i.e., the thin layer covers the substrate) due to the misfit strain [26].

In QWR growth, one of the important parameters is the relative strain energy Λ (e.g., [26,27]). Namely, the ratio of the strain energy change relative to the constant strain energy in the wetting layer due to the misfit strain over the constant strain energy, as defined below

$$\begin{aligned} \Lambda &\equiv \frac{W - \frac{1}{2}\int_V C_{ijkl}\gamma^*_{ij}\gamma^*_{kl}\,\mathrm{d}V}{\frac{1}{2}\int_V C_{ijkl}\gamma^*_{ij}\gamma^*_{kl}\,\mathrm{d}V} \\ &= \frac{\frac{1}{2}\int_\Gamma t_i u_i\,\mathrm{d}\Gamma - \frac{1}{2}\int_\Gamma t_k^{(fw)} u_k\,\mathrm{d}\Gamma}{\frac{1}{2}\int_V C_{ijkl}\gamma^*_{ij}\gamma^*_{kl}\,\mathrm{d}V}, \end{aligned} \tag{32}$$

where Λ is also called the relative strain energy, which will be numerically examined in the next section. We remark that while various energetic parameters were introduced for characterizing defect dynamics [28], this relative strain energy has been successfully applied in the prediction of new QWR formation and QWR array patterns under the Stranski–Krastanow growth mode [26,27,29].

4. Numerical examples

Before applying our solution to examine the strain energy in QWR system, we have first checked our program for the reduced cases with existing solutions [24]. We found

that our solution can be reduced exactly to the existing exact closed-form results [24]. Other numerical tests have also been carried out, all showing that our solution and program are correct. Therefore, after validation, we now apply our solution to calculate the relative strain energy and the distribution of the strain energy density. We remark that while our BEM formulation can be applied to more complicated situations, here we only study the reduced case where the QWR is free-standing on or embedded in the half-plane substrate. The half-plane model is reduced from our bimaterial result by setting the upper half-plane ($z>0$) with very low material stiffness as compared to the lower half-plane substrate. (The material stiffness in the upper half-space is equal to 10^{-10} times the material stiffness in the lower half-space.)

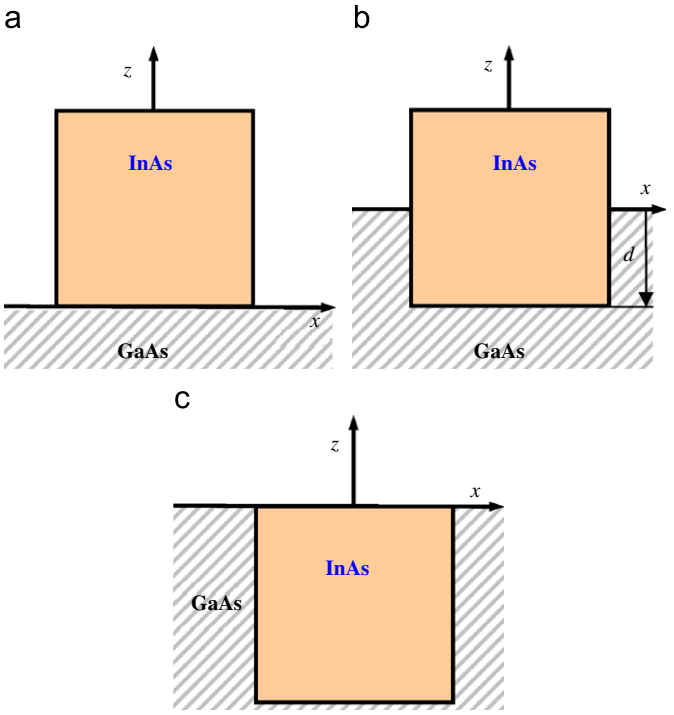

Fig. 2. Geometry of a square InAs QWR on or inside the GaAs substrate. Shown in (a) to (c) are the three special cases: namely, totally free-standing (a), half free-standing (half-in and half-out in (b)), and fully embedded (c).

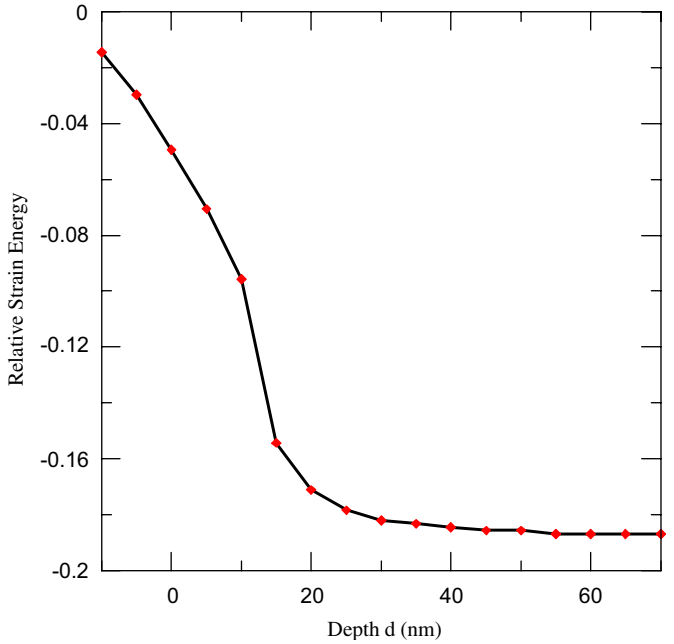

Fig. 3. Variation of relative strain energy with depth of a square QWR.

4.1. Variation of relative strain energy with QWR depth

We first apply our bimaterial BEM program to study the problem where a square InAs (1 1 1) QWR growing on a GaAs (1 1 1) substrate (Fig. 2). The material properties of InAs and GaAs in the (1 1 1)-direction are obtained by coordinate transform from those in the (0 0 1)-directions [30]. The QWR has a dimension of 20 nm × 20 nm and a uniform misfit strain field $\gamma^*_{xx}=\gamma^*_{yy}=\gamma^*_{zz}=0.07$. The boundary condition on the surface of the substrate is assumed to be traction-free. While a total free-standing

Table 1
Variation of relative strain energy with base angle of the isosceles triangle of InAs (1 1 1) QWR, which is free-standing on the GaAs (1 1 1) substrate

Base angle (°)	Relative strain energy
30	−5.88E − 03
37	−6.91E − 03
45	−7.90E − 03
52	−8.70E − 03
60	−9.76E − 03
67	−1.11E − 02
75	−1.43E − 02

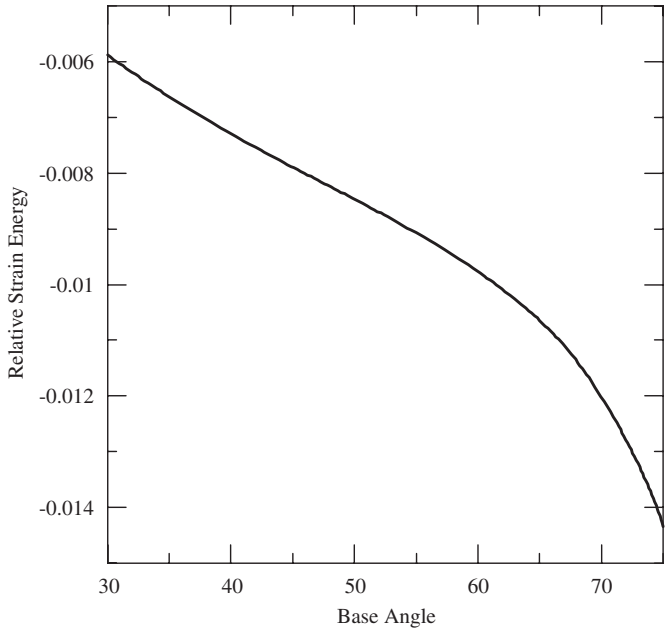

Fig. 4. Variation of relative strain energy with base angle of isosceles triangle of InAs (1 1 1) QWR, which is free-standing on the GaAs (1 1 1) substrate.

QWR on the substrate is illustrated in Fig. 2(a), a fully embedded QWR is shown in Fig. 2(c). We let d be the depth of the QWR, measured from the bottom side of the QWR to the surface of substrate (Fig. 2(b)). We then calculate the relative strain energy (i.e., Eq. (32)) of the QWR as a function of depth d, varying from -10 nm (Fig. 2(a)) to 70 nm, at the interval of 5 nm. Fig. 3 shows clearly that with increasing depth d, the magnitude of the relative strain energy increases, reaching the value when the QWR is within an infinite substrate ($=-0.19$). In other words, bringing an embedded QWR to the surface will decrease the relative strain energy. This is true since with increasing surface area of the QWR to the air, more surface energy will be released, resulting in small relative strain energy. This important feature could represent the competition between the surface and bulk energies, i.e. [31,32], and should be particularly interesting to epitaxial growth.

4.2. Effect of QWR shape on relative strain energy and distribution of strain energy density

We assume now that there is an isosceles triangle of InAs (1 1 1) QWR, free-standing on the GaAs (1 1 1) substrate. The base angle of the triangle varies from 30° to 75° while the area of triangle maintains the same. The misfit strain is again uniform, i.e. $\gamma^*_{xx}=\gamma^*_{yy}=\gamma^*_{zz}=0.07$. The boundary condition on the surface of the substrate is traction-free. Both the relative strain energy and strain energy density in the QWR are investigated.

The relative strain energy for the triangular QWR with different base angles are listed in Table 1and its variation with the base angle are also shown in Fig. 4. It is observed that the magnitude of the relative strain energy increases with increasing base angle of the QWR triangle. In other words, the steeper the QWR is, the larger the magnitude of the relative strain energy becomes.

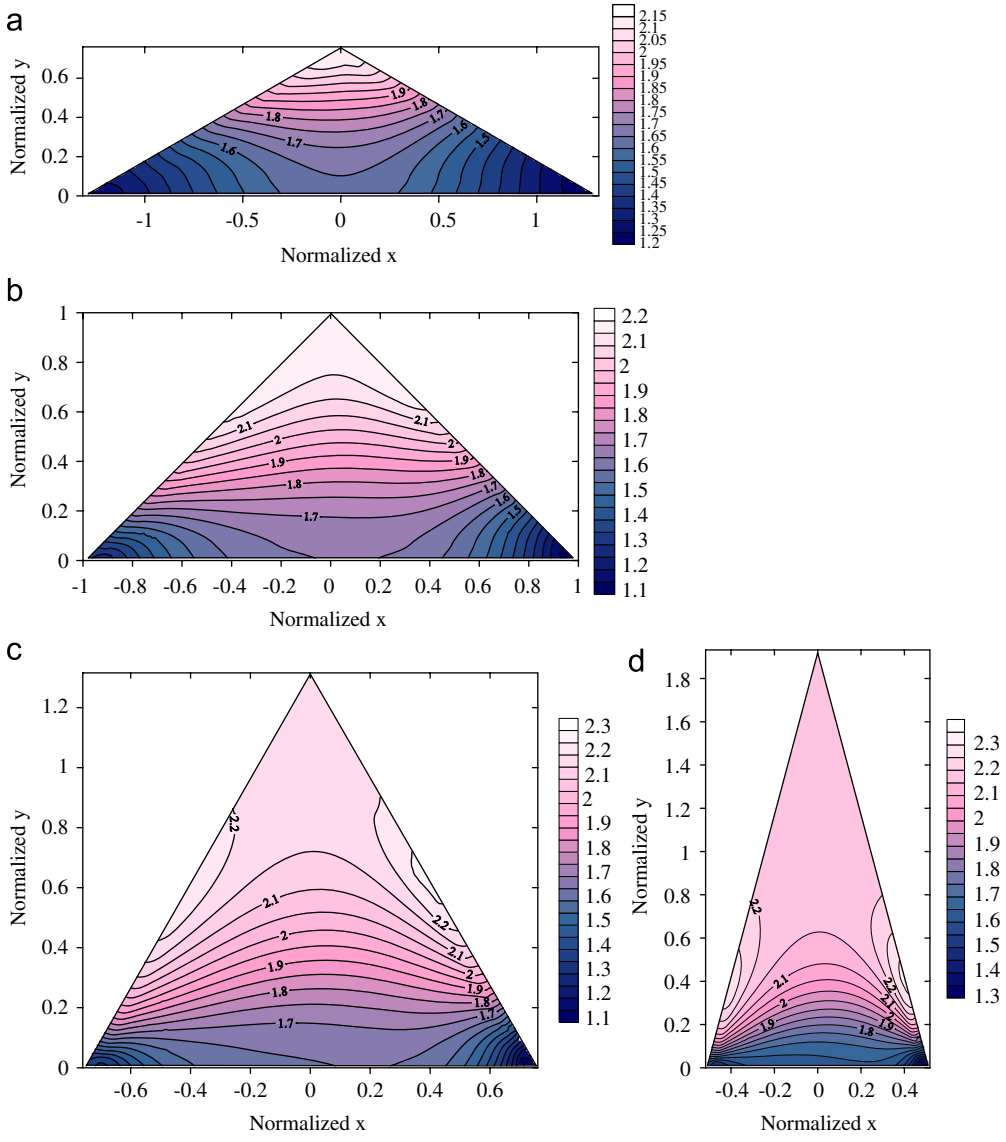

Fig. 5. Contours of strain energy density (10^9 kg/ms^2) in isosceles triangle of InAs (1 1 1) QWR with base angle 30° (a), 45° (b), 60° (c), and 75° (d).

The contours of the strain energy density for these free-standing triangular QWRs are plotted in Fig. 5. It is clear that the strain energy density distribution is strongly influenced by the QWR shape. Particularly at the locations near the vertex and base corners, the strain energy densities are quite different among these triangles. We further observed that the strain energy density near the vertex is larger than those near the base corners. The magnitude of strain energy density increases roughly from 2.15 to 2.35 (10^9 kg/ms^2) as the base angle varies from 30° to 75°.

5. Conclusions

In the paper, we first derive the bimaterial Green's functions in anisotropic elastic media in terms of the elegant Stroh formalism. The corresponding BEM formulation is then presented. Since the involved Green's functions are in exact closed forms, the kernel integration can be analytically carried out for the constant element discretization. After testing our bimaterial BEM program for various reduced simple cases, we then apply our program to calculate the strain energy density and the relative strain energy in InAs (1 1 1) QWR free-standing on or embedded in GaAs (1 1 1) substrate. Our numerical results showed that, for the case of an isosceles triangle of InAs (1 1 1) QWR on the substrate, the strain energy density within the QWR strongly depends on the base angle of the triangle. We also observed that the magnitude of the relative strain energy for this case increases with increasing base angle. For a square QWR either free-standing on or embedded in the substrate, we found that the magnitude of the relative strain energy increases with increasing depth of the QWR in the substrate, which represents the competition between the surface and bulk energies. Our numerical examples also demonstrate the significant influence of the QWR shape and location on both the strain energy density and the relative strain energy in the QWR, which should be particularly useful to the successful growth of QWRs via epitaxial approach.

Acknowledgments

This work was supported by Defense Threat Reduction Agency Joint Science and Technology Office (DTRA-JSTO) under the Grant W911NF-06-2-0038. The two reviewers provided helpful comments on the initial version of the manuscript.

Appendix A. Expression of matrix $\boldsymbol{Q}$

We assume that the source point is in the half-plane of material λ ($\lambda = 1$ or 2). Then $\boldsymbol{Q}$ can be expressed as

$$Q_{rk}^{\lambda\lambda,v} = K_{rj}^{\lambda\lambda}(I_v)_j \overline{A}_{kj}^{\lambda} \tag{A.1}$$

if the field point is in the half-plane of material λ, and

$$Q_{rk}^{\lambda\mu,v} = K_{rj}^{\lambda\mu}(I_v)_j A_{kj}^{\lambda} \tag{A.2}$$

if the field point is in the other half-plane of material μ ($\mu \neq \lambda$). In Eqs. (A.1) and (A.2), the matrix $\boldsymbol{K}$ is given by

$$\boldsymbol{K}^{\lambda\lambda} = (\boldsymbol{A}^{\lambda})^{-1}(\boldsymbol{M}^{\lambda} + \overline{\boldsymbol{M}}^{\mu})^{-1}(\boldsymbol{M}^{\mu} - \overline{\boldsymbol{M}}^{\lambda})\overline{\boldsymbol{A}}^{\lambda},$$

$$\boldsymbol{K}^{\lambda\mu} = (\boldsymbol{A}^{\mu})^{-1}(\boldsymbol{M}^{\mu} + \overline{\boldsymbol{M}}^{\lambda})^{-1}(\boldsymbol{M}^{\lambda} + \overline{\boldsymbol{M}}^{\lambda})\boldsymbol{A}^{\lambda}, \tag{A.3}$$

with $\boldsymbol{M}^{\lambda} = -\mathrm{i}\boldsymbol{B}^{\lambda}(\boldsymbol{A}^{\lambda})^{-1}$ ($\lambda = 1$ or 2) and the diagonal matrix I_v has the following expression for different indexes v:

$$I_1 = \mathrm{diag}[1,0,0]; \quad I_2 = \mathrm{diag}[0,1,0]; \quad I_3 = \mathrm{diag}[0,0,1]. \tag{A.4}$$

References

[1] Bimberg D, Grundmann M, Ledentsov NN. Quantum dot heterostructures. New York: Wiley; 1998.
[2] Caro LD, Tapfer L. Strain and piezoelectric fields in arbitrarily oriented semiconductor heterostructures. Phys Rev B 1995;51:4381–7.
[3] Ross FM, Tersoff J, Tromp RM. Coarsening of self-assembled Ge quantum dots on Si (0 0 1). Phys Rev Lett 1998;80:984–7.
[4] Daruka I, Tersoff J, Barabasi AL. Shape transition in growth of strained islands. Phys Rev Lett 1999;82:2753–6.
[5] Davies JH. Elastic field in a semi-infinite solid due to thermal expansion or a coherently misfitting inclusion. ASME J Appl Mech 2003;70:655–60.
[6] Yang B, Pan E. Elastic fields of quantum dots in multilayered semiconductors: a novel Green's function approach. J Appl Mech 2003;70:161–8.
[7] Pan E, Han F. Strain fields in InAs/GaAs quantum wire structures: inclusion versus inhomogeneity. J Appl Phys 2005;98:013534.
[8] Ding HJ, Chen WQ, Jiang AM. Green's functions and boundary element method for transversely isotropic piezoelectric materials. Eng Anal Bound Elements 2004;28:975–87.
[9] Pan E, Amadei B. Boundary element analysis of fracture mechanics in anisotropic bimaterials. Eng Anal Bound Elements 1999;23:683–91.
[10] Pan E. A BEM analysis of fracture mechanics in 2-D anisotropic piezoelectric solids. Eng Anal Bound Elements 1999;23:67–76.
[11] Garcia F, Saez A, Dominguez J. Anisotropic and piezoelectric materials fracture analysis by BEM. Comput Struct 2005;83:804–20.
[12] Groh U, Kuna M. Efficient boundary element analysis of cracks in 2D piezoelectric structures. Int J Solids Struct 2005;42:2399–416.
[13] Qin QH. 2D Green's functions of defective magnetoelectroelastic solids under thermal loading. Eng Anal Bound Elements 2005;29:577–85.
[14] Lee KY, Kwak SG. Determination of stress intensity factors for bimaterial interface stationary rigid line inclusions by boundary element method. Int J Fract 2002;113:285–94.
[15] Salvadori A. A symmetric boundary integral formulation for cohesive interface problems. Comput Mech 2003;32:381–91.
[16] Sun Y, Zhang Z, Kitipornchai S, Liew KM. Analyzing the interface between collinear interfacial cracks by an efficient boundary element-free method. Int J Eng Sci 2006;44:37–48.
[17] Giannopoulos GI, Anifantis NK. A BEM analysis for thermo-mechanical closure of interfacial cracks incorporating friction and thermal resistance. Comput Meth Appl Meth Eng 2007;196:1018–29.
[18] Garcia F, Rojas-Diaz R, Saez A, Zhang Ch. Fracture of magnetoelectroelastic composite materials using boundary element method (BEM). Theor Appl Fract Mech 2007;47:192–204.
[19] Lei J, Wang YS, Gross D. Dynamic interaction between a subinterface crack and the interface in a bi-material: time-domain BEM analysis. Arch Appl Mech 2003;73:225–40.
[20] Lei J, Wang YS, Gross D. Time-domain BEM analysis of a rapidly growing crack in a bi-material. Int J Fract 2004;126:103–21.

[21] Lei J, Wang YS, Gross D. Two dimensional numerical simulation of crack kinking from an interface under dynamic loading by time domain boundary element method. Int J Solids Struct 2007;44:996–1012.
[22] Ting TCT. Anisotropic elasticity: theory and applications. New York: Oxford University Press; 1996.
[23] Mura T. Micromechanics of defects in solids. Dordrecht: Martinus Nijhoff; 1987.
[24] Pan E. Eshelby problem of polygonal inclusions in anisotropic piezoelectric full- and half-planes. J Mech Phys Solids 2004;52:567–89.
[25] Pan E. Mindlin's problem for an anisotropic piezoelectric half space with general boundary conditions. Proc R Soc London 2002;458: 181–208.
[26] Holy V, Springholz G, Pinczolits M, Bauer G. Strain induced vertical and lateral correlations in quantum dot superlattices. Phys Rev Lett 1999;83:356–9.
[27] Stangl J, Holy V, Bauer G. Structural properties of self-organized semiconductor nanostructures. Rev Mod Phys 2004;76: 725–83.
[28] Phillips R. Crystals, defects, and microstructures: modeling across scales. New York: Cambridge University Press; 2001.
[29] Yang B, Tewary VK. Formation of a surface quantum dot near laterally and vertically neighboring dots. Phys Rev B 2003;68: 035301.
[30] Pan E, Albrecht JD, Zhang Y. Elastic and piezoelectric fields in quantum wire semiconductor structures—a boundary integral equation analysis. Phys Status Solidi B 2007;244:1925–39.
[31] Pao CW, Srolovitz DJ. Stress and morphology evolution during island growth. Phys Rev Lett 2006;96:186103.
[32] Pao CW, Srolovitz DJ. Atomistic simulation of stress evolution during island growth. J Mech Phys Solids 2006;54:2527–43.